Design study of a radio-frequency quadrupole for high-intensity beams *

Jungbae Bahng[1] Eun-San Kim[2;1)] Bong-Hyuk Choi[3]

[1] Department of Physics, Kyungpook National University, Daegu 41566, Republic of Korea
[2] Department of Accelerator Science, Graduate School, Korea University Sejong campus, Sejong 30019, Republic of Korea
[3] Institute for Basic Science, Daejeon 34047, Republic of Korea

Abstract: The Rare isotope Accelerator Of Newness (RAON) heavy-ion accelerator has been designed for the Rare Isotope Science Project (RISP) in Korea. The RAON will produce heavy-ion beams from 660-MeV-proton to 200-MeV/u-uranium with continuous wave (CW) power of 400 kW to support research in various scientific fields. Its system consists of an ECR ion source, LEBTs with 10 keV/u, CW RFQ accelerator with 81.25 MHz and 500 keV/u, a MEBT system, and a SC linac. In detail, the driver linac system consists of a Quarter Wave Resonator (QWR) section with 81.25 MHz and a Half Wave Resonator (HWR) section with 162.5 MHz, Linac-1, and a Spoke Cavity section with 325 MHz, Linac-2. These linacs have been designed to optimize the beam parameters to meet the required design goals. At the same time, a light-heavy ion accelerator with high-intensity beam, such as proton, deuteron, and helium beams, is required for experiments. In this paper, we present the design study of the high intensity RFQ for a deuteron beam with energies from 30 keV/u to 1.5 MeV/u and currents in the mA range. This system is composed of an Penning Ionization Gauge ion source, short LEBT with a RF deflector, and shared SC Linac. In order to increase acceleration efficiency in a short length with low cost, the 2nd harmonic of 162.5 MHz is applied as the operation frequency in the D^+ RFQ design. The D^+ RFQ is designed with 4.97 m, 1.52 bravery factor. Since it operates with 2nd harmonic frequency, the beam should be 50% of the duty factor while the cavity should be operated in CW mode, to protect the downstream linac system. We focus on avoiding emittance growth by the space-charge effect and optimizing the RFQ to achieve a high transmission and low emittance growth. Both the RFQ beam dynamics study and RFQ cavity design study for two and three dimensions will be discussed.

Keywords: heavy-ion accelerator, RFQ accelerator, high intensity, RFQ beam dynamics, RFQ cavity design

PACS: 29.20.Ej **DOI:** 10.1088/1674-1137/41/7/077002

1 Introduction

The Rare isotope Accelerator Of Newness (RAON) heavy-ion accelerator has been designed as a facility for the Rare Isotope Science Project (RISP). RAON will produce 400 kW continuous wave (CW) rare-isotope beams, from proton to uranium beams, using the In-Flight Fragment (IF) system [1]. The main accelerator in RAON consists of an electron cyclotron resonance (ECR) ion source, low-energy beam transport systems (LEBTs), radio frequency quadrupole (RFQ), medium-energy beam transport (MEBT) system, and linear accelerators, namely Linac-1 and Linac-2. The main RFQ has been designed to accelerate dual-charge-state beams ($^{238}U^{33+}$ and $^{238}U^{34+}$) from 10 keV/u to 500 keV/u with 81.25 MHz. Linac-1 consists of 21 Quarter Wave Resonator (QWR) cavities (β_g=0.047) of 81.25 MHz and 80 Half Wave Resonator (HWR) cavities (β_g=0.12) of 162.5 MHz. Linac-2 consists of 69 Superconducting Spoke (SSR-1) cavities ($\beta_g = 0.3$) of 325 MHz and 78 SSR-2 cavities ($\beta_g = 0.53$) of 325 MHz. Researchers in various scientific fields require high-intensity light-ion beams, of current greater than 15 mA, at target. To achieve RISP's objectives, a high-intensity light-ion beam injector is required as the main injector system has been designed to accelerate massive ion beams, such as uranium, and it is unable to accelerate proton beams at currents greater than 1 mA. In order to avoid the space-charge effect, which dominates in the low-energy region, it is determined that the high-intensity ion beam energy should be increased from 30 keV/u to 1.5 MeV/u. The injector consists of a short LEBT system with two solenoids to match the beam parameters required by the RFQ accelerator, a deflector, and a collimator to control the beam intensity, as shown in Fig. 1. We propose an RF deflector and 2nd harmonic operation frequency RFQ [2] to reduce the cavity size and length, and increase the acceleration efficiency by using a high surface electric field.

Received 16 December 2016, Revised 09 March 2017
∗ Supported by Korea University Future Research Grant
1) E-mail: eskim1@korea.ac.kr
©2017 Chinese Physical Society and the Institute of High Energy Physics of the Chinese Academy of Sciences and the Institute of Modern Physics of the Chinese Academy of Sciences and IOP Publishing Ltd

Figure 2 shows that the output beam energy per length is dependent on the RFQ operation frequency [3–16].

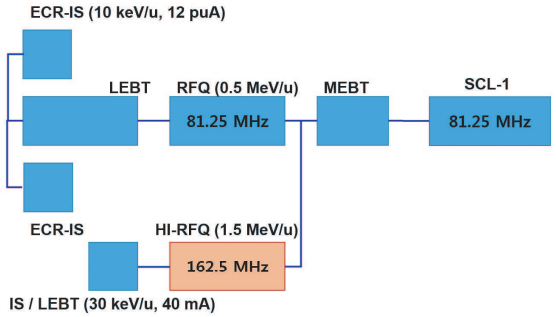

Fig. 1. Layout of the RAON injector system.

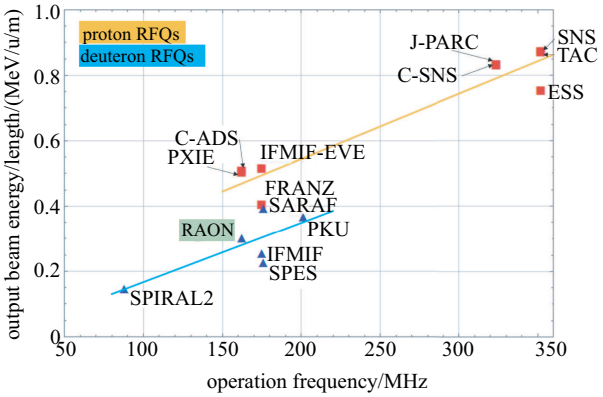

Fig. 2. (color online) Proton and deuteron RFQs worldwide.

W. Kilpatrick showed that discharge in a vacuum depends on the frequency, as in the following formula [17]:

$$f = 1.643 \times E_{\rm k}^2 {\rm e}^{-8.5/E_{\rm k}}, \quad (1)$$

where f is the operation frequency [MHz], and $E_{\rm k}$ is the peak surface electric field [MV/m]. As shown in Eq. (1), the second harmonic RFQ could be designed with an increment of 35% at maximum surface electric field for the case of 81.25 MHz. Moreover, as the cross-sectional area is smaller at higher resonance frequencies, less material could be used for manufacturing the part. Since Kilpatrick criterion scaling is used for the RFQ design and bravery factors are typically chosen between 1.5 and 2.0, a higher operation frequency can give the advantage of high-efficiency acceleration. Thus, we adopted 162.5 MHz as the HI-RFQ operation frequency.

A conceptual schematic diagram is presented in Fig. 3. An RF deflector and collimator remove 50% of the beam by deflected strength difference. The LEBT system is optimized to capture 50% of the ion beam by confirming the offset distance and beam size. By using the RF deflector, the side effects of beam loss in Linac-1 will be minimized. So far, we have studied the second harmonic RFQ with deflector. Increasing the operation frequency yields the advantages of reducing the cavity size in terms of resonant space, and allowing a cavity design with high electric field by the Kilpatrick effect. To meet the minimum current requirement of 15 mA and an economical structure, the RFQ frequency was chosen to be twice the frequency of the linac operation frequency, and the beam intensity was chosen to be 40 mA.

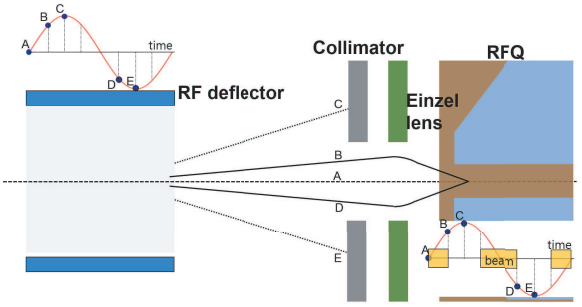

Fig. 3. Schematic diagram of 2nd harmonic RFQ.

2 Beam dynamics design

The RAON RFQ design parameters are presented in Table 1. The main RFQ has been developed to accelerate heavy-ion beams, such as uranium, at low intensity [18, 19]. The RFQ is focused on minimizing the longitudinal emittance to obtain a large acceptance in the SC Linac. In contrast, the D^+ RFQ has been designed to accelerate high intensity beams. In order to avoid the large space-charge effect due to low velocity and high beam intensity, the RFQ has a short gentle buncher section and reasonable transmission rate. A deuteron beam with 40 mA and large transverse emittance, 0.25(n.r.) mm-mrad, is used for the RFQ design. Since high current causes a large space-charge effect, beams blow up easily, thereby increasing emittance. The deuteron beam is generated from the ion source and transported by the LEBT with an energy of 30 keV/u. The RFQ accelerates the deuteron beam to 1.5 MeV/u. The goals of the high-intensity RFQ beam dynamics study are to minimize the RFQ length and emittance growth and to optimize a high transmission rate. The fundamental objective regarding the RFQ is to design a beam with acceptable longitudinal bunching at the entrance of the linac. PARMTEQM [20] code, which was developed at Los Alamos National Laboratory, is used to generate the RFQ design parameters. We consider the RFQ to be operated at 162.5 MHz and a deuteron beam of 40 mA (peak) with 50% duty rate to be accelerated. We designed the RFQ to have a low longitudinal emittance, thus avoiding transverse emittance growth, as well as a high transmission rate and short length. Figure 4 contains various parameters. B is the focusing strength, m is the modulation factor, V is the vane voltage (kV), ϕ is the phase in degrees, and $W_{\rm syn}$ is

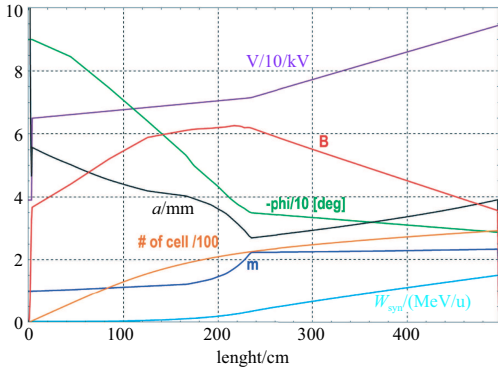

Fig. 4. (color online) D^+ RFQ design parameters.

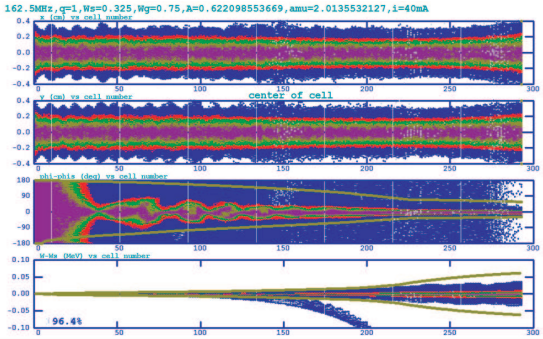

Fig. 5. (color online) Result of the dynamics of D^+ RFQ design.

the energy of a synchronous particle. To optimize the RFQ design, we adopted a ramped vane voltage, slowly increased the modulation factor in the shaper section, simultaneously increased the synchronous phase in the acceleration section, and adjusted the focusing strength across the entire region, as shown in Fig. 4. In order to minimize the input focusing parameter, α in the Twiss parameters, we reduce the vane voltage in the radial matching (RM) section. Since the inflection point at the end of the RM section is due to reduction of vane voltage in the RM section, the vane voltage was modified to be proportional to the second order in the RM section and modulations in shape were varied smoothly in the shaper section. The synchronous phase becomes $-35°$ at the end of the gentle buncher section and $-28°$ at the end of the acceleration section in order to avoid the space-charge effect. Since the RFQ design parameters were optimized, it was possible to obtain advantages such as length reduction and high transmission rate, as shown in Fig. 5. A transmission rate of 96.4% was obtained for a beam intensity of 40 mA. The output beam distributions are presented in Fig. 6. The rms beam size and beam divergence are obtained, respectively, as 1.38 mm and 8.45 mrad for horizontal, and 1.31 mm and 7.32 mrad for vertical beam distributions. The longitudinal phase and energy spread are obtained as 7.26° and 8 keV/u, as shown in Fig. 6. Figure 7 describes the beam loss position along the beam axis. The particle losses occur largely at the end of the gentle buncher section for large space-charge effect and at the energy allowance limit of PARMTEQ simulation. The total loss is 3.6% as we mentioned in Table 1.

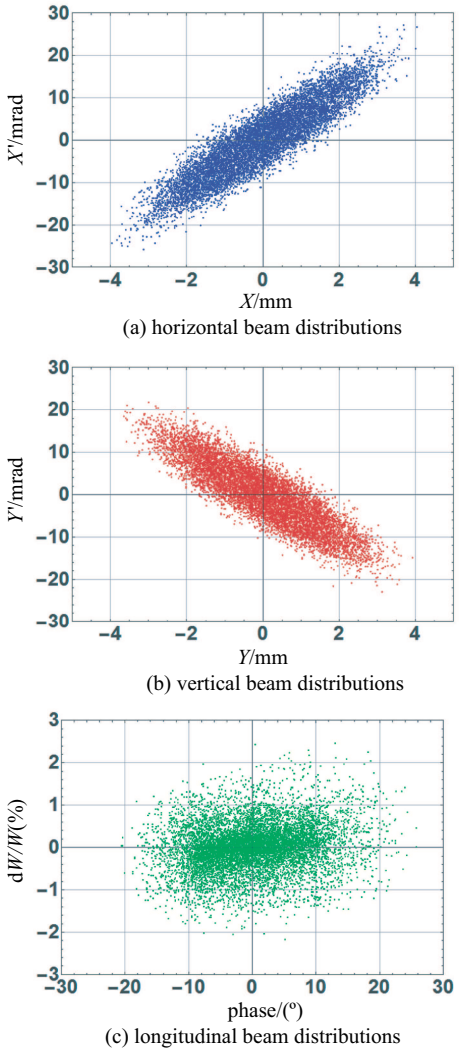

Fig. 6. (color online) D^+ Beam distributions at the end of the RFQ.

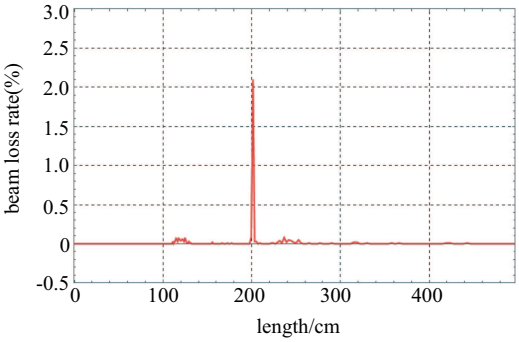

Fig. 7. (color online) Beam loss rate along the beam axis in the RFQ.

Table 1. RAON RFQ design parameters.

particle	D^+	$^{238}U^{33.5+}$
Q/A	1/2	1/7.1
frequency/MHz	162.5	81.25
input beam energy/(MeV/u)	0.03	0.01
output beam energy/(MeV/u)	1.5	0.50
peak beam current/mA	40	0.40
vane voltage/kV	65.0–94.4	50.0–138.0
length/cm	496.8	498.0
transmission rate(%)	96.4	97.7
input emittance (n.r.)/mm·mrad	0.25	0.12
max. surface field/(MV/m)	20.6	17.9
bravery factor	1.52	1.70

Table 2. Beam parameters in the D^+ RFQ.

emittance(n.r)	input	output
horizontal/mm·mrad	0.25	0.2886
vertical/mm·mrad	0.25	0.2672
longitudinal/mm·mrad	CW	0.3098
/(keV/u-deg)		56.77
α_x	1.066	-2.082
α_y	1.066	1.772
β_x/(cm/rad)	7.498	37.629
β_y/(cm/rad)	7.498	37.200

The RFQ beam parameters are given in Table 2, and the transverse and longitudinal emittances are shown in Fig. 8. The initial transverse emittance is assumed to be 0.25 mm-mrad, owing to the emittance growth caused by large beam current. The beam parameters at the entrance of the RFQ are calculated from the beam dynamics design of the RFQ such that α is 1.066 and β is 7.498 cm/rad. The output beam parameters are used as input beam parameters in the SC Linac downstream of the RFQ. The beam dynamics in the SC Linac depend on the emittance ratio of ϵ_Z/ϵ_T, which is related to the space-charge effect, emittance growth, halo formation, and acceleration efficiency. If there is a small emittance ratio of ϵ_Z/ϵ_T at the exit from the RFQ, for example, 0.5, the emittance growth and halo effect in the SC Linac are large. On the other hand, if the emittance ratio is large, for instance, 2.0, the beam dynamics of large beam loss and low acceleration efficiency are obtained [21]. In order to calculate the emittance ratio, the units of the longitudinal emittance can be converted by

$$\epsilon_{W,\Phi}[\text{MeV}\cdot\text{deg}]=\Delta W\cdot\Delta\Phi \tag{2}$$

$$\epsilon_{W,t}[\text{eV}\cdot\text{s}]=\frac{\epsilon_{W,\Phi}[\text{MeV}\cdot\text{deg}]}{360\cdot f[\text{MHz}]} \tag{3}$$

$$\epsilon_z[\text{mm}\cdot\text{mrad}]=\frac{\epsilon_{W,t}[\text{eV}\cdot\text{s}]\times c}{\gamma m_0 c^2[\text{MeV}]}, \tag{4}$$

where f is the RFQ frequency, γ is the Lorentz factor of the particle, c is the speed of light, and m_o is the rest mass of the particle. We designed the RFQ to have $\epsilon_Z/\epsilon_T=1.07$ to optimize the acceleration efficiency and avoid emittance growth due to the space-charge effect, as shown in Table 2 and Fig. 8. Transverse emittances of 15% and 6.8% were increased by currents of 40 mA and 20 mA, respectively.

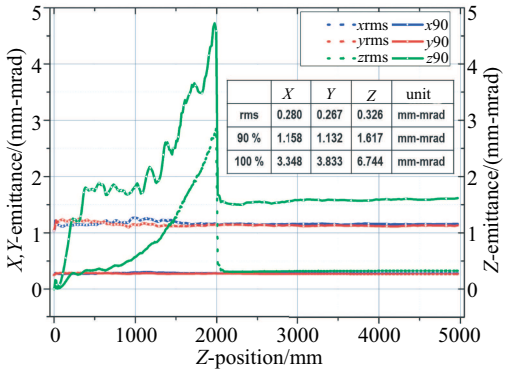

Fig. 8. (color online) Beam emittances in the D^+ RFQ.

3 Error analysis

The RFQ transmission efficiency depends on the RFQ design parameters. The RFQ system is bound by tight tolerances for the fabrication, field error, beam parameter mismatches from the LEBT, unexpected beam emittance, particle energy offset, and installation misalignment. To set tolerance limits on the various parameters of the RFQ and to understand the real operation status of the RFQ, an error analysis study was performed. The study of the error analysis was carried out with PARMTEQM code. Figure 9 shows various effects in the case of breaking out errors. The acceptance criterion is taken as a transmission rate of 95%. Based on this criterion, the tolerance limits are set for the various parameters. The transverse emittances for the x and y directions are kept constant during the error analysis for the displacement and divergence simulation. The transverse particle displacement is restricted to 500 μm and the divergence is ±10 mrad. Particles with energy deviation of −0.75 keV/u to +0.3 keV/u from synchronicity can be accelerated in the RFQ while satisfying the criterion. Beam parameter tolerances of ± 0.426 (α), −1.5−3.0 cm/rad (β), and +0.13 mm-mrad (n.r.) are acceptable.

4 Two-dimensional cavity design

One quadrant of the RFQ cavity was designed and simulated by the SUPERFISH [22] code, and the structure parameters were optimized for a design frequency of 161 MHz. It was decided to design the frequency to be lower than the resonant frequency owing to manufacturing errors. The vane structures were optimized to

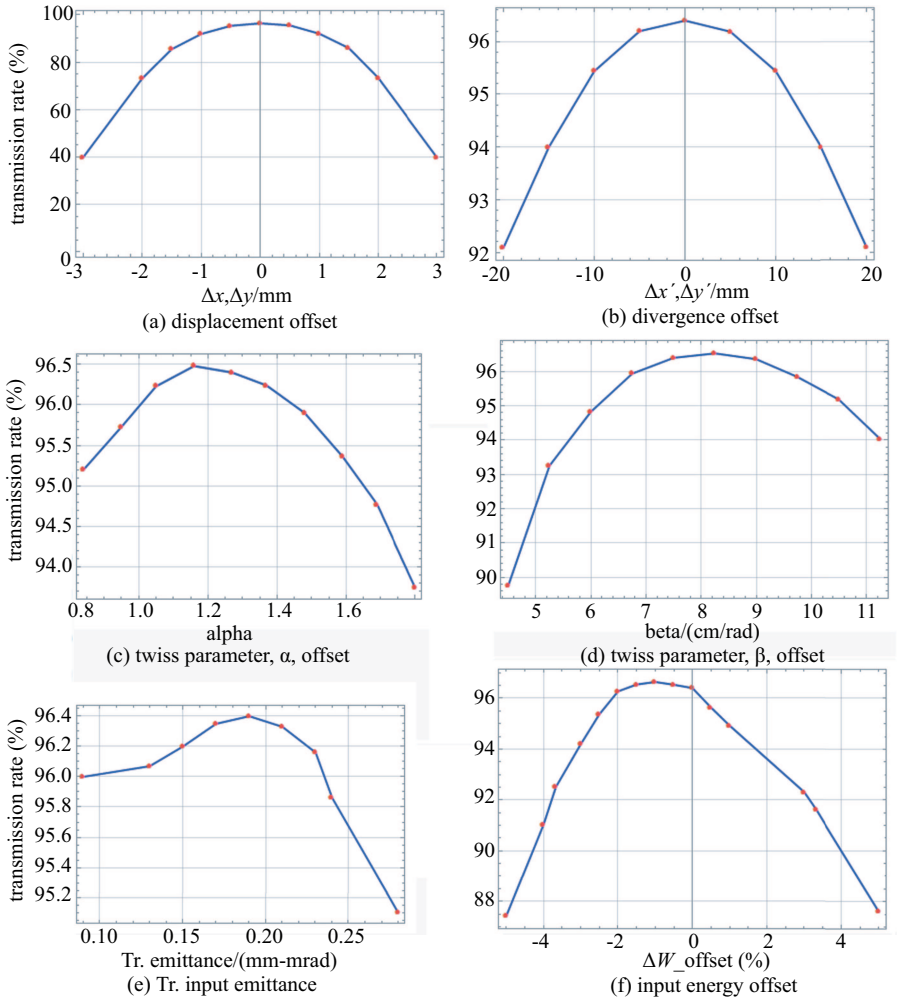

Fig. 9. Results of the error analysis.

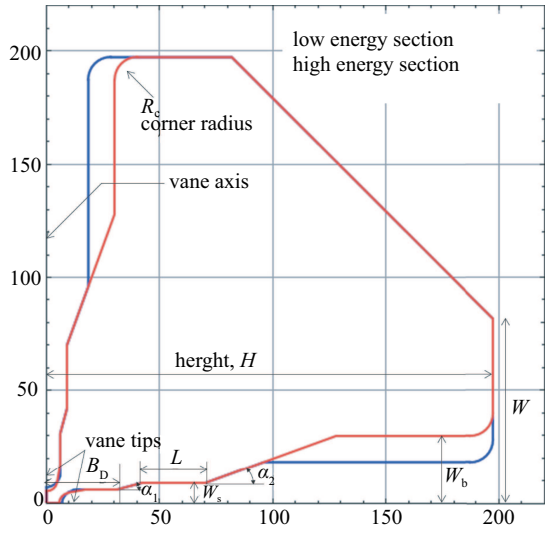

Fig. 10. Design of vane quadrant for the D^+ RFQ.

minimize the power dissipation, and to maximize the quality factor (Q-factor) and the difference between the quadrupole and dipole mode frequencies. Low power dissipation results in easy cooling. A high Q-factor indicates slow energy loss relative to the stored energy and low power dissipation. We designed the vane structure to have a high Q-factor at the resonant frequency. The ideal vane for obtaining the highest Q-factor is hyperbolic; however, it is difficult to fabricate. Figure 10 shows the cross-section of one quadrant of the RFQ cavity and the definition of parameters of the geometrical vane structure. The red line indicates the vacuum space of the vane in the low-energy section, and the blue line indicates the high-energy section. The quadrant structure of the RFQ cavity was designed with a radius of curvature of 0.90 times the bore radius. The detailed geometrical parameters are listed in Table 3.

The position elements of the vane-tip are defined as shown in Fig. 11 [22]. Here, r_0 is the average bore radius, ρ is the vane-tip transverse radius of curvature, $\alpha_{\rm bk}$ is a breakout angle of 10° for the tool bit cutting the vane, $B_{\rm W}$ is the half-width of the vane blank, $B_{\rm D}$ is the vane blank depth, that is, the distance from the RFQ axis

to the vertex of angle α_1, W_s is the half-width of the shoulder, L_s is the shoulder segment of length, and α_2 is the vertex of the angle between the shoulder and vane base, W_b. Figure 12 shows the vane structures along the RFQ. The red line indicates the horizontal vanes, and the blue line indicates the vertical vanes. Both the horizontal and vertical vanes were designed with a fringe-field region of 11.18 mm, radial matching gap of 11.22 mm, radial matching section of 37.01 mm, and total length, acceleration length, of 4967 mm. The vanes are designed with a fringe field gap of 6.35 mm and vane length of 4949.94 mm for the horizontal side and a fringe field gap of 6.05 mm and vane length of 4950.24 mm for the vertical side. Moreover, the vane-tip sensitivity can be calculated by SUPERFISH code. We obtained the highest vane-tip sensitivity of 5.4 MHz/mm. In order to achieve 1 % stability, a tolerance of 30 μm would be required for vane-tip alignment and manufacturing.

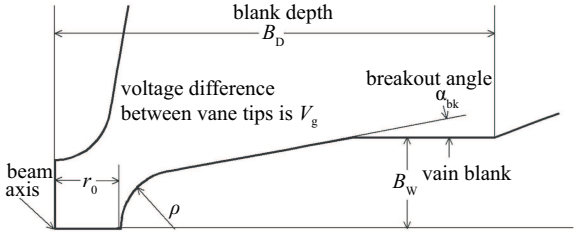

Fig. 11. Schematic diagram of vane-tip geometry.

Table 3. Geometrical parameters of the RFQ cavity.

parameters	values
breakout angle, α_{bk}/(°)	10
blank half-width, B_w/cm	0.6
blank depth, B_D/cm	3.1
α_1/(°)	15
shoulder half-width, W_s/cm	0.9
shoulder length, L_s/cm	2.8
α_2/(°)	20
base half width, W_b/cm	3.0
height, H/cm	20.0

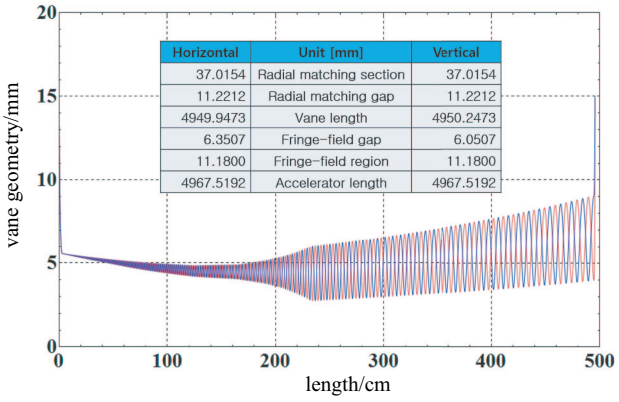

Fig. 12. Vane structure along the D^+ RFQ.

By using these geometrical parameters, we obtained a well-matched design resonant frequency of the quadrupole (TE_{210}) mode. After setting these parameters, the adjacent resonant frequency, dipole mode (TE_{110}), was investigated near the quadrupole mode by applying appropriate boundary conditions. For the quadrupole mode, the Neumann boundary condition was applied to the upper and right edges and the Dirichlet boundary condition was applied to lower and left edges. On the other hand, the left edge was changed according to the Neumann boundary condition for the dipole mode. The frequency of the adjacent dipole mode was obtained as 156.5 MHz, as shown in Fig. 13, and the Q-factor for the quadrupole mode was obtained 15126. Although the difference between the quadrupole and dipole modes is larger than 420 times the bandwidth, 10.7 kHz, we need to study the mode analysis by 3D simulation, as the simulation was performed with the two-dimensional (2D) SUPERFISH code. The peak power consumption in one quadrant was calculated to be 31 kW from SUPERFISH. Thus, the total average power consumption is related to the 2D result from SUPERFISH through the relation [23]:

$$P_{\rm total}=P_{\rm SF}\cdot\alpha_{\rm 3D}\cdot\alpha_{\rm v}+P_{\rm beam}, \tag{5}$$

where $\alpha_{\rm 3D}=1.3$ is a factor that accounts for the 3D losses, i.e. a simulation compensation of 20 %, and a RF transmission loss of 10 %, $P_{\rm beam}$ is the average beam power of 59 kW at 40 mA of a peak beam current with 50 % of duty rate while the cavity is operated in CW mode, and $\alpha_{\rm v}=1.1^2=1.21$ accounts for an inter-vane voltage margin of up to 10 %. We obtained an average power consumption for RF amplifier as 255 kW by sum of average beam power. Since rapid rising and falling are difficult in 81.25 MHz operation of the RF amplifier, the RFQ cavity operates in CW mode while 50% duty rate of beam is accelerated. The estimated peak powers of the required RF amplifier and RFQ cavity are 315 kW and 195 kW for the RFQ cavity, respectively.

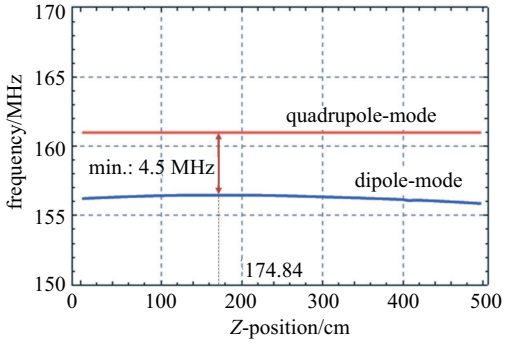

Fig. 13. Adjacent mode of the D^+ RFQ resonant frequency.

This is the problem of errors and allowance in cavity construction. In order to compensate for fabrication errors, we adopted a tuner system to tune the resonant frequency of the RFQ cavity. When the tuners are inserted into the RFQ cavity, the resonant frequency is increased. By changing the tuner depth, the resonant frequency is controlled to the designed value. The tuner radius was chosen to be 30 mm based on the standard CF-flange size. The various resonant frequencies were obtained by different tuner depths and the tuning sensitivity was 200 kHz/mm in both the low- and high-energy sections, as shown in Fig. 14.

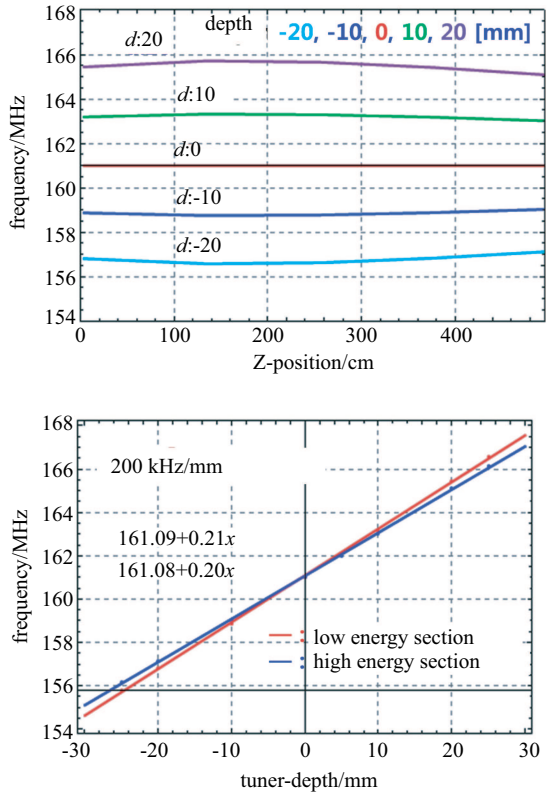

Fig. 14. (color online) Result of tuner simulation.

5 Three-dimensional cavity design

In order to understand the required electromagnetic field distributions from beam dynamics in detail, a three-dimensional (3D) RF analysis was carried out using CST Microwave Studio code [24]. The resonance of the RFQ cavity generates an electromagnetic field distribution as desired and an unexpected TEM mode and field deformation due to the complex structure [25]. In general, a longitudinal magnetic field is induced in an RFQ cavity and should be parallel to both the entrance and exit plates. The vane cutback is designed to solve the boundary value problem [9]. The cutback was designed using CST code to maintain the resonant frequency of 161.0 MHz. The detailed design parameters are presented in Table 4 and their definitions are shown in Fig. 15. The cutback system affects the field distributions due to space for the magnetic flux path. It causes a difference in heat distribution on the cutback geometry. We focus the maximum temperature on the cutback geometry while maintaining the resonance frequency, which is related to the height and depth of the cutback system. The resonance frequency of 161.0 MHz is obtained with the desired operation mode, TE210 in the cutback system. Figure 16 shows the 3D modeling of the cutback system and Fig. 17 shows the electric and magnetic field distributions at the operation mode. The left-hand figure shows the electric field distributions by cutting across the vanes of RFQ cavity and the right-hand figure shows the magnetic field distributions with a side-view in the RFQ cavity.

Table 4. Geometrical parameters of the cutback.

parameters	Case-1	Case-2	Case-3	Case-4	Case-5
slope angle, θ/(°)	0	0	0	0	0
height, $h1$/mm	197.3	197.3	197.3	197.3	197.3
low	energy	section			
height, $h2$/mm	40.0	80.0	120.0	140.0	160.0
depth, d/mm	112.4	113.1	126.6	136.7	152.4
gap, g/mm	11.2	11.2	11.2	11.2	11.2
high	energy	section			
height, $h2$/mm	40.0	80.0	120.0	140.0	160.0
depth, d/mm	104.8	108.7	111.8	119.9	134.0
gap, g/mm	6.4	6.4	6.4	6.4	6.4

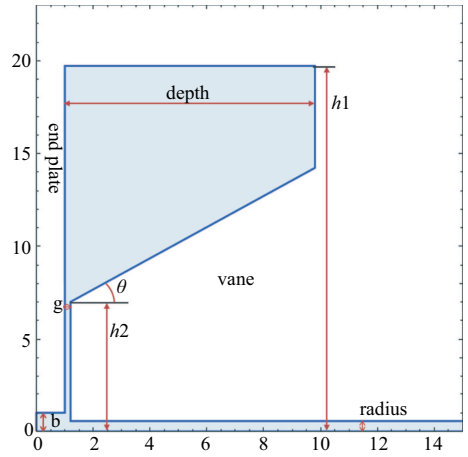

Fig. 15. Definitions of cutback system.

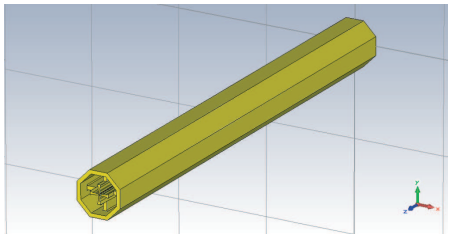

Fig. 16. 3D model of the D^+ RFQ cavity with cutback system.

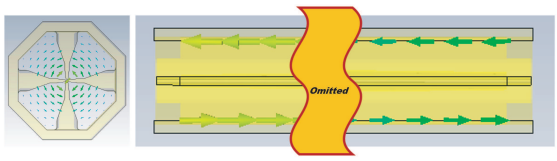

Fig. 17. (color online) Electric (left) and magnetic (right) field distributions.

We obtained the RFQ cavity resonance frequency with various cutback systems, as presented in Table 5. The cutback height affects the resonance frequency. The resonance frequency requires a large difference between the desired operation mode TE210 and the unwanted mode. These results imply that the adjacent resonance frequency depends on the height of the cutback system. As we mentioned, the cutback affects the field distributions owing to the difference in resonance space. The magnetic field distributions along the beam axis with $x=60.0$ mm, $y=60.0$ mm offsets from the cavity centre in the horizontal and vertical directions are described as shown in Fig. 18. The cutback system influences the EM field distributions and thermal distributions. However, the field distributions are tunable by the tuner position; we focus on the temperature distribution results of various cutback systems. For the thermal analysis, the ambient temperature is set as 27 °C as room temperature and a heat source is applied from the CST EM field distribution. The applied input power is 195 kW, which is cavity loss power multipled by a scale factor. In order to understand the effects of the cutback model, cooling systems are not applied in these simulations. The maximum temperatures for various cutback models are presented in Fig. 19. The maximum temperature is located in the cutback region due to strong magnetic field and surface current. The values decreases with the height of the cutback system; however, the change of maximum temperature increases when the height is over 140 mm. Therefore, we choose the Case-4 model with a cutback height of 140 mm. By applying proper cutback height, we can minimize the maximum temperature in the vane as shown in Fig. 19. The undercut parameters such as depth and height are determined by optimizing resonance frequency, thermal distributions and EM field distribution. In the case of a thin vane like Case-1, the electromagnetic field strength is similar to the thick vane case. However, as the copper volume in the undercut region is small, it results in a high temperature in the undercut system. In the case of a thick vane like Case-5, the maximum temperature is similar to result of Case-4, but a deep undercut is required to maintain the operation frequency of 162.5 MHz. Our undercut system is optimized in terms of easy manufacturing and maximum temperature in the undercut region. In the present design, we achieved a maximum temperature of 314 °C and average temperature of 110 °C without the cooling system. However, a cooling system for the RFQ cavity is necessary to avoid the shift of resonance frequency by thermal increases. Therefore, based on the present design results, we will plan to design a tuning system to obtain the resonance frequency of 162.5 MHz by tuning, as well as a cooling system for the RFQ cavity for high power operation.

Table 5. Adjacent modes of D^+ RFQ resonant frequency [MHz] and Max. temperature from CST simulation.

parameters	Case-1	Case-2	Case-3	Case-4	Case-5
D-mode/MHz	155.6	155.7	155.7	155.7	155.8
D-mode/MHz	157.5	157.7	157.7	157.7	157.8
Q-mode/MHz	161.0	161.0	161.0	161.0	161.0
Q-mode/MHz	162.3	162.3	162.3	162.3	162.3
D-mode/MHz	166.6	166.6	166.8	166.8	166.8
Max.Temp./	844.9	585.7	333.7	314.0	331.8

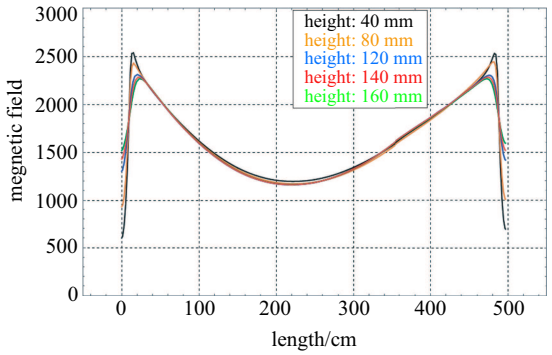

Fig. 18. (color online) Longitudinal magnetic field distributions at $x=60$, $y=60$ mm, with various cutback models.

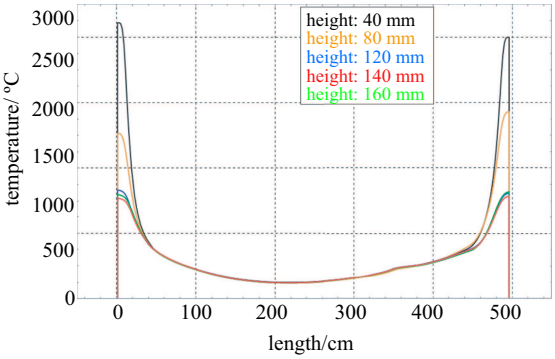

Fig. 19. (color online) Result of temperature distribuions at $x=0$, $y=10$ mm, with various cutback models.

6 Summary and future plan

A high-intensity RFQ accelerator for RAON was designed to optimize the transmission rate and minimize the RFQ length, beam loss, and emittance growth. The

RFQ operation frequency was chosen to be 162.5 MHz to minimize the RFQ size, while the beam intensity was increased to 40 mA of peak beam current with 50% of duty rate to achieve the required current of 15 mA at the target. We considered that an RFQ has a transverse-to-longitudinal emittance raito of 1.07 to avoid emittance growth. An RFQ beam dynamics study was performed with the PARMTEQM code. With this optimization, a high transmission rate of 96.4% and an emittance growth of 15% were achieved. A 2D EM analysis of the RFQ was conducted with the SUPERFISH code. Since rapid rising and falling are difficult in 81.25 MHz operation of the RF amplifier, the cavity operates in CW mode while 50% pulse beam is accelerated by the RFQ cavity. A power consumption of 195.0 kW and average Q-factor of 15126 were obtained for the RFQ cavity with quadrupole mode. To investigate the 3D EM properties, cutback design was performed to achieve a resonant frequency with various heights and depths of the cutback system. Finally, a resonance frequency of 161.0 MHz was obtained from a 3D simulation using CST code and the adjacent dipole mode was obtained as 157.7 MHz, which is far from the 3.3 MHz frequency of the quadrupole mode. This value is less than the 2D simulation result but it is more reasonable. In order to avoid the closed adjacent dipole modes, a dipole stabilizer rod will be installed in the endplate, since 1.3 MHz of mode separation is obtained in 3D simulation. The adjacent resonance frequency, field distributions, and temperature distribution depend on the cutback geometry. Since the field distribution could be controlled by the tuner, the maximum temperature is taken into account in the cutback system design. Based on the dependence between maximum temperature and cutback height, we select 140 mm of cutback height. Since the maximum temperature is obtained as 314 ℃ and the average temperature is around 110 ℃ without a cooling system, cooling of the RFQ cavity is necessary to avoid resonance frequency shift by increasing temperature. Based on the present design result, we plan to design a tuning system to obtain 162.5 MHz of resonance frequency by a tuner as well as a cooling system for the RFQ cavity for high power operation.

References

1 RAON Accelerator and Experimental System Technical Design Report, September 30, 2013
2 J. Bahng et al, *Proceedings of IPAC2015, MOPTY025*, Richmond, USA, 2015
3 C. Zhang, A. Schempp, Nuclear Instruments and Methods in Physics Research A, **586**: 153–159 (2008)
4 J. Staples, "RFQ Progress", presentation at Project X collaboration Meeting at LBNL (April 10-12, 2012)
5 A. Pisent et al, *Proceedings of EPAC08*, THPP078, Genoa, Italy, 2008
6 Z. Zhang et al, *Proceedings of LINAC2012*, THPB039, Tel-Aviv, Israel, 2012
7 H. F. Ouyang, S. Fu, *Proceedings of LINAC2006*, THP070, Knoxville, Tennessee, USA, 2006
8 Y. Kondo, K. Hasegawa, T. Morishita, R. A. Jameson, Physical Review Special Topics - Accelerators and Beams, **15**: 080101 (2012)
9 R. Gaur, P. Shrivastava, Journal of Electromagnetic Analysis and Applications, **2**: 519–528 (2010)
10 A. Caliskan, H. F. Kisoglu, M. Yilmaz, Nuclear Science and Techniques, **26**: 030103 (2015)
11 ESS Technical Design Report, April 22, 2013
12 RFQ Final Report, technical note SPIRAL2 EDMS-I-004532
13 A. Pisent et al, *Proceedings of EPAC2008*, THPP078, Genna, Italy, 2008
14 M. Marchetto et al, *Proceedings of EPAC2004*, TUPLT066, Lucerne, Switzerland, 2004
15 J. Rodnizki, Z. Horvits, *Proceedings of LINAC2010*, TUP045, Tsukuba, Japan, 2010
16 Y. R. Lu et al, Physics Procedia, **60**: 212–219 (2014)
17 W. D. Kilpatrick, The Review of Scientific Instruments, **28**(10): 1957
18 E. S. Kim et al, Nuclear Instruments and Methods in Physics Research A, **794**: 215–223 (2015)
19 B. S. Park et al, *Proceedings of IPAC2016*, TUPMR030, Busan, Korea, 2016
20 K. R. Crandall, T. P. Wangler, L. M. Young, J. H. Billen, G. H. Neuschaefer, and D. L. Schrage, RFQ Design Codes, LA-UR-96-1836
21 N. Solyak, A. Vostrikov, Project X Front-end concept for 162.5 MHz RFQ, Project X-doc-816-v1, 2011
22 J. H. Billen and L. M. Yong, Poisson Superfish, LA-UR-96-1834
23 A. Pisent et al, *Proceedings of EPAC2008*, THPP078, Genoa, Italy, 2008
24 CST Studio Suite, CST Microwave Studio, 2012, http://www.cst.com/
25 R. Romanov et al, *Proceedings of ICAP09*, THPSC047, San Francisco, CA, USA, 2009